Engineered spin-state transitions of two interacting electrons in semiconductor nanowire quantum dots

Yan-Ting Chen and Shun-Jen Cheng*
Department of Electrophysics, National Chiao Tung University, Hsinchu 30010, Taiwan, Republic of China

Chi-Shung Tang†
Department of Mechanical Engineering, National United University, Miaoli 36003, Taiwan, Republic of China
(Received 9 December 2009; revised manuscript received 25 March 2010; published 11 June 2010)

Spin properties of two interacting electrons in a quantum dot (QD) embedded in a nanowire with controlled aspect ratio and longitudinal magnetic fields are investigated by using a configuration-interaction (CI) method. The developed CI theory based on a three-dimensional parabolic model provides explicit formulations of the Coulomb matrix elements and allows for straightforward and efficient numerical implementation. Our studies reveal fruitful features of spin-singlet-triplet transitions of two electrons confined in a nanowire QD, as a consequence of the competing effects of geometry-controlled kinetic-energy quantization, Coulomb interaction, and spin-Zeeman energy. The developed theory is further employed to study various spin states of two quantum-confined electrons in the regime of "crossover" dimensionality, from quasi-two-dimensional (disklike) QDs to finite one-dimensional (rodlike) QDs.

DOI: 10.1103/PhysRevB.81.245311 PACS number(s): 73.21.La, 71.45.Gm, 71.15.−m, 71.70.Ej

I. INTRODUCTION

Stimulated by recent success in coherent control of two-electron (2e) spin in laterally coupled quantum dots (QDs),[1] the spin states of two interacting electrons in semiconductor QDs have received increasingly considerable attention. Accessible and engineerable spin states of few electrons in QDs thus have become one of the basic features required by the quantum information applications in which electron spins are utilized as quantum bit.[2,3] For two-dimensional (2D) epitaxial QDs, magnetic field induced spin-singlet-triplet (ST) transitions of 2e ground states have been studied extensively for years.[4–7] The underlying physics of the ST transitions is usually associated with the energetic competition between quantized kinetic energies, the Coulomb interaction, and spin-Zeeman energies. Reversely switching the singlet and triplet spin states of a lateral 2e QD is feasible by utilizing electrical control.[8] Moreover, it has been both theoretically and experimentally shown that more complex oscillating spin states can be generated either by reducing the lateral confinement or by increasing an applied magnetic field.[9–12]

Recently, the local-gate electrical depletion[13–15] and the bottom-up grown techniques[16,17] have been developed for the fabrication of few-electron QDs embedded in a nanowire. These experimental developments open up an opportunity of exploring the *crossover* mechanisms from the 2D (disklike) to the finite one-dimensional (1D) (rodlike) QD regimes. Such nanowire QDs (NWQDs) are advantageous for geometrical control over a wide rage of aspect ratio a (typically from $a \sim 10^{-1}$ to $a \gg 1$).[16,17] The excellent versatility of shape and dimensionality makes NWQDs a suitable nanomaterial for scalable quantum electronics. Very recently, successful fabrication of single-electron transistors made of InAs-based gate-defined NWQDs and observations of the singlet-triplet transitions of two electrons in the QDs have been demonstrated.[18] How the highly tunable longitudinal confinement of NWQD affects and can be utilized to tailor the spin properties of few electrons in NWQDs are interesting subjects worth studying.

The above experimental efforts motivate us to perform a theoretical investigation of the spin states of two electrons in InAs-based NWQDs (Ref. 18) by using a configuration-interaction (CI) method based on a three-dimensional (3D) parabolic model.[19] The developed CI theory is applicable for cylindrically symmetric QDs with arbitrary transverse and longitudinal confinement strengths[20–22] and provides explicit generalized formulation of the Coulomb matrix, and thus allows for straightforward and efficient numerical or even semianalytical implementation widely applicable for various cylindrically symmetric QDs. Our CI studies of 2e charged NWQDs with controlled geometric aspect ratios and longitudinal magnetic fields reveal fruitful features of spin ST transitions, as a consequence of the competing effects of geometry-engineered kinetic-energy quantization, Coulomb interaction, and spin-Zeeman energy. The developed theory is further employed to explore the spin-state diagram of the two quantum-confined electrons in the regime of "crossover" dimensionality from quasi-2D (disklike) QDs to finite 1D (rodlike) QDs.

This paper is organized as follows: Sec. II describes the theoretical model and the developed configuration-interaction theory for few-electron problems of three-dimensionally confining quantum dots. In Sec. III, we present and discuss the calculated results of the magnetoenergy spectra, the ST transitions, and the geometry-engineered spin-state diagrams of 2e-charged quantum dots embedded in nanowires. Concluding remarks are presented in Sec. IV.

II. MODEL

A. Single-particle model

We begin with the problem of a single electron in a NWQD with a uniform longitudinal magnetic field **B**

$=(0,0,B)$, which is described by the single-electron Hamiltonian,

$$H_0 = \frac{1}{2m^*}(\mathbf{p} + e\mathbf{A})^2 + V_c(x,y,z) + H_Z. \quad (1)$$

Here the first term indicates the term of kinetic energy with $\mathbf{A}=(B/2)(-y,x,0)$ being the vector potential in symmetric gauge, m^* the effective mass of electron, and e the charge of an electron. The second term is the confining potential of NWQD modeled by

$$V_c(x,y,z) = \frac{1}{2}m^*[\omega_0^2(x^2+y^2) + \omega_z^2 z^2] \quad (2)$$

with ω_0 and ω_z parametrizing, respectively, the transverse and the longitudinal confining strength. The last term is the spin-Zeeman energy $H_Z=g^*\mu_B B s_z$, in terms of the z component of electron spin $s_z=\pm 1/2$, the effective Lande g factor of electron g^*, and the Bohr magneton μ_B. The single-particle Hamiltonian (1) leads to the extended Fock-Darwin single-particle spectrum,

$$\epsilon_{n,m,q,s_z} = \hbar\omega_+\left(n+\frac{1}{2}\right) + \hbar\omega_-\left(m+\frac{1}{2}\right) + \hbar\omega_z\left(q+\frac{1}{2}\right) + E_Z, \quad (3)$$

where $n,m,q=0,1,2,\ldots$ denote oscillator quantum numbers, $E_Z=g^*\mu_B B s_z$ is the spin-Zeeman energy, $\omega_\pm = \omega_h \pm \omega_c/2$ are in terms of the hybridized frequency $\omega_h \equiv (\omega_0^2+\omega_c^2/4)^{1/2}$ and the cyclotron frequency $\omega_c=eB/m^*$. The corresponding eigenstate $|n,m,q\rangle$ possesses the orbital angular momentum projection $\ell_z=\hbar(n-m)$ and the parity $P=1$ $(P=-1)$ with respect to z axis for an even (odd) q number. The wave function of the lowest orbital is given by

$$\psi_{000}(\mathbf{r}) = [(2\pi)^{3/4} l_h \sqrt{l_z}]^{-1} \times \exp\left[-\frac{1}{4}\left(\frac{x^2+y^2}{l_h^2} + \frac{z^2}{l_z^2}\right)\right] \quad (4)$$

with the characteristic lengths of the wave function extents $l_h=\sqrt{\hbar/2m^*\omega_h}$ and $l_z=\sqrt{\hbar/2m^*\omega_z}$. The wave functions of other excited states can be generated by successively applying the following defined raising operators:[19]

$$a^\dagger = \frac{1}{\sqrt{2}}\left[\frac{x+iy}{2l_h} - l_h(\partial_x + i\partial_y)\right],$$

$$b^\dagger = \frac{1}{\sqrt{2}}\left[\frac{x-iy}{2l_h} - l_h(\partial_x - i\partial_y)\right],$$

$$a_z^\dagger = \frac{z}{2l_z} - l_z\partial_z \quad (5)$$

onto the ground state $|0,0,0\rangle$, i.e.,

$$|n,m,q\rangle = \frac{(\hat{a}^\dagger)^n(\hat{b}^\dagger)^m(\hat{a}_z^\dagger)^q}{\sqrt{n!m!q!}}|0,0,0\rangle. \quad (6)$$

The diameter of cross section of bottom-up synthesized nanowire is typically ~50–70 nm. By contrast, the length of a QD in a nanowire, defined by imposed electrodes or heterostructure potential barriers, is highly tunable over a wide range from 10 to 300 nm.[17] For characterizing the geometry of a NWQD, it is convenient to define the parameter of aspect ratio,

$$a \equiv \frac{l_z}{l_0} = \sqrt{\frac{\omega_0}{\omega_z}} \quad (7)$$

according to the characteristic length of the lowest-orbital wave function based on the 3D parabolic model. A rodlike (disklike) NWQD is characterized by the value of aspect ratio $a>1$ $(a<1)$, where the longitudinal extent of the electron wave function is longer (shorter) than the transverse one on the cross section of the nanowire. Notably, the effective aspect ratio $a=l_z/l_0$ defined here is not but very close to the geometric aspect ratio a_{geom}, namely, $a \simeq a_{\text{geom}}=\mathbf{L}_z/\mathbf{L}_0$ with $\mathbf{L}_0$ $(\mathbf{L}_z)$ being the cross-section diameter (length) of NWQD. Figure 1 presents the calculated single-electron energy spectrum as a function of aspect ratio a for a NWQD with fixed lateral confinement $\hbar\omega_0=13.3$ meV at zero magnetic field according to Eq. (3). The chosen parameter of lateral confinement $\hbar\omega_0=13.3$ meV is determined by fitting the numerically calculated energy separation between the two lowest single-electron orbitals of a cylindrical InAs/InP NWQD of cross-section diameter $\mathbf{L}_0=65$ nm by 3D finite-difference simulation. In the simulation, the Schrödinger equation for a single electron confined in a 3D cylindrical potential well is solved by using finite-difference method with the used parameters: the effective mass $m^*=0.023m_0$ of electron for InAs and the InAs/InP band-edge offset $V_b=0.6$ eV as the barrier height of the confining potential.[17,23]

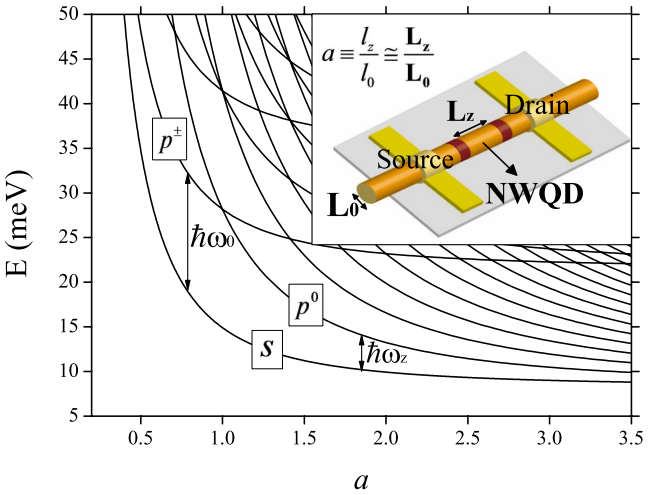

FIG. 1. (Color online) Single-electron energy spectrum as a function of aspect ratio a of a NWQD with fixed lateral confinement $\hbar\omega_0=13.3$ meV at zero magnetic field obtained from the 3D parabolic model. The considered lateral confinement strength $\hbar\omega_0=13.3$ meV corresponds to the cross-section diameter $\mathbf{L}_0\sim 65$ nm for a cylindrical InAs nanowire. The low-lying s, $p^\pm$, and p^0 orbitals are relevant to a 2e problem. The energy quantization for a short (long) NWQD with $a<1$ $(a>1)$ is characterized by the energy difference between the lowest and first excited orbitals $\hbar\omega_0$ $(\hbar\omega_z)$.

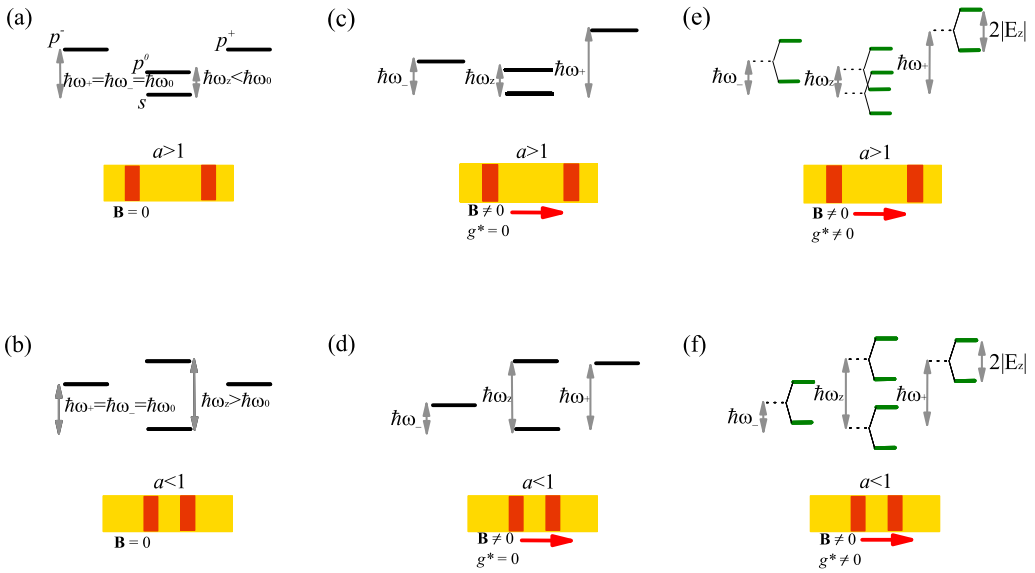

FIG. 2. (Color online) Schematic illustration of the electronic structures, consisting of few relevant low-lying orbitals (one s and three p orbitals), of [(a), (c), and (e)] long rodlike NWQDs and [(b), (d), and (f)] short disklike NWQDs with or without longitudinal magnetic field B and including or excluding the spin-Zeeman splitting E_Z ($g^*=0$ or $g^*\neq 0$). (a) $a>1$ and $B=0$; (b) $a<1$ and $B=0$; (c) $a>1$, $B\neq 0$, and $g^*=0$; (d) $a<1$, $B\neq 0$, and $g^*=0$; (e) $a>1$, $B\neq 0$, and $g^*\neq 0$; and (f) $a<1$, $B\neq 0$, and $g^*\neq 0$.

In a 2e problem, the most relevant orbitals are the two lowest ones because the kinetic-energy difference between the two orbitals is the main energy cost, in competition with the Coulomb or spin-Zeeman energies, for a spin-triplet state to be the 2e ground state. By convention, we from now on name the lowest single-electron state $|n,m,q\rangle=|0,0,0\rangle$ as s orbital and the next three p-shell states $|0,0,1\rangle$, $|1,0,0\rangle$, and $|0,1,0\rangle$ as p^0, p^+, and p^- orbitals, respectively. According to Eq. (3), the energy of the lowest s orbital is explicitly given by

$$\epsilon_{s,s_z}=\frac{1}{2}(\hbar\omega_+ + \hbar\omega_- + \hbar\omega_z) + g^*\mu_B B s_z \tag{8}$$

and those of the three p-shell orbitals are, respectively, given by

$$\epsilon_{p^0,s_z}=\epsilon_{s,s_z}+\hbar\omega_z,$$

$$\epsilon_{p^+,s_z}=\epsilon_{s,s_z}+\hbar\omega_+,$$

$$\epsilon_{p^-,s_z}=\epsilon_{s,s_z}+\hbar\omega_-. \tag{9}$$

For $B=0$, we have $\epsilon_{s,s_z}=\hbar\omega_0(1+1/2a^2)$, $\epsilon_{p^0,s_z}=\epsilon_{s,s_z}+\hbar\omega_0/a^2$, and $\epsilon_{p^+,s_z}=\epsilon_{p^-,s_z}=\epsilon_{s,s_z}+\hbar\omega_0$ according to Eqs. (7) and (9). Here, the p^+ and p^- orbitals are degenerate with the same energy separation from the s orbital, $\hbar\omega_\pm=\hbar\omega_0$ while the p^0 orbital is energetically higher than s orbital by $\hbar\omega_z=\hbar\omega_0/a^2$. Obviously, p^0 ($p^\pm$) is the second lowest orbital for a long (short) NWQD with $a>1$ ($a<1$) at zero magnetic field, as shown in Fig. 1. For a symmetric NWQD with $a=1$, the p^0 and $p^\pm$ orbitals form a threefold orbital-degenerate shell. Figure 2(a) or Fig. 2(b) schematically depicts the low-lying orbitals of a long (short) NWQD with $a>1$ ($a<1$) at zero magnetic field.

Applying a longitudinal magnetic field onto a cylindrical NWQD breaks the degeneracy of p^+ and p^- orbitals. The orbital Zeeman effect lowers (raises) the energy level of the $p^-(p^+)$ orbital from $\hbar\omega_0$ to $\hbar\omega_-$ ($\hbar\omega_+$). Thus, if a long NWQD is subjected to a sufficiently strong magnetic field, the second lowest orbital of the dot could be changed from the p^0 to p^-. By contrast, the second lowest orbital of a short NWQD is always the p^- orbital. Therefore, the characteristic energy quantization of the p^- orbitals, $\hbar\omega_-=\hbar(\omega_0^2+\omega_c^2/4)^{1/2}-\hbar\omega_c/2$, is often a key parameter for a short NWQD or a moderately long NWQD with strong magnetic field. Considering wide-band-gap materials such as GaAs, the g factors are usually small and the spin-Zeeman effect on the energy shift of orbital is negligible. Figure 2(c) or Fig. 2(d) depicts the B-dependent electronic orbitals of a long (short) NWQDs, where vanishing spin-Zeeman splitting is assumed ($g^*=0$ is set).

For a low-energy gap material with larger g^*, such as InAs, the spin-Zeeman effect could be significant in the spin ST transition of 2e QD. Figure 2(e) or Fig. 2(f) schematically shows the spin-resolved electronic orbitals of a long (short) NWQDs with $B\neq 0$ and $g^*\neq 0$ by the spin-Zeeman splitting $2E_Z$. With the spin-Zeeman effect, all the spin-up (spin-down) orbitals are energetically lowered (raised) by $E_Z=g^*\mu_B B/2$ according to Eq. (3). If the applied magnetic field or the g factor of material is so large that the spin-Zeeman splittings exceed the kinetic-energy quantization of QD, both of the two lowest single-electron states are the spin-up ones and the ground state of the 2e dot is ensured to be a spin-triplet state simply according to spin Pauli exclusion principle.

In this work, the following formulation for the effective g factor for an electron confined in InAs-based QD is adopted,[17,24,25]

$$g^* = g\left[1 - \frac{P^2}{3}\frac{\Delta_{\rm SO}}{E_g^{\rm eff}(E_g^{\rm eff}+\Delta_{\rm SO})}\right], \tag{10}$$

where $E_g^{\rm eff}$ is the effective energy gap of semiconductor QD, $g=2.0$ is the Lande g factor for free electron, $\Delta_{\rm SO}$ is the spin-orbit splitting in the valence band, and P is the parameter of interband transition matrix element.[24]

Here, the effective energy gap of a QD can be estimated as $E_g^{\rm eff}=E_g^{\rm bulk}+\epsilon_{s,s_z}$, where $E_g^{\rm bulk}$ is the bulk energy gap and ϵ_{s,s_z} is the quantization energy of the lowest electronic orbital of the QD with $B=0$ measured from the conduction-band edge. For InAs-based QDs, we take the following parameter values: $E_g^{\rm bulk}=460$ meV, $\Delta_{\rm SO}=390$ meV, and $P^2=21.5$ eV.[17] Accordingly, the value of g^* for a symmetric NWQD with $\mathbf{L}_0=\mathbf{L}_z=65$ nm is estimated as large as $g^* \approx -11$.[17]

B. Interacting few-electron model

The interacting Hamiltonian of few electrons in a NWQD can be expressed in the form of second quantization as

$$H = \sum_{i,\sigma} \epsilon_{i\sigma} c_{i\sigma}^\dagger c_{i\sigma} + \frac{1}{2}\sum_{ijkl,\sigma\sigma'} \langle ij|V|kl\rangle c_{i\sigma}^\dagger c_{j\sigma'}^\dagger c_{k\sigma'} c_{l\sigma}, \tag{11}$$

where i,j,k,l denote the composite indices of single-electron orbitals such as $|i\rangle=|n_i,m_i,q_i\rangle$, $c_{i\sigma}^\dagger$ $(c_{i\sigma})$ the electron creation (annihilation) operators, and $\sigma=\pm$ the electron spins $s_z=\pm\frac{1}{2}$. The first (second) term on the right-hand side of Eq. (11) represents the kinetic energy of electrons (the Coulomb interactions between electrons) and the Coulomb matrix elements are defined as

$$\langle ij|V|kl\rangle \equiv \frac{e^2}{4\pi\varepsilon_0\kappa}\int\int d\mathbf{r_1}d\mathbf{r_2}\psi_i^*(\mathbf{r_1})\psi_j^*(\mathbf{r_2}) \times \frac{1}{|\mathbf{r_1}-\mathbf{r_2}|}\psi_k(\mathbf{r_2})\psi_l(\mathbf{r_1}), \tag{12}$$

where κ is the dielectric constant of dot material and ε_0 the permittivity in free space. For InAs material, we take $\kappa=15.15$. After lengthy derivation, one can obtain the generalized Coulomb matrix elements for the case of $a \geq 1$,

$$\begin{aligned}\langle n_i m_i q_i; n_j m_j q_j|V|n_k m_k q_k; n_l m_l q_l\rangle = {} & \left(\frac{1}{\pi l_h}\right)\frac{\delta_{R_L,R_R}\cdot\delta_{q_i+q_j+q_l+q_k,\rm even}}{\sqrt{n_i!m_i!q_i!n_j!m_j!q_j!n_k!m_k!q_k!n_l!m_l!q_l!}} \\ & \times \sum_{p_1=0}^{\min(n_i,n_l)}\sum_{p_2=0}^{\min(m_i,m_l)}\sum_{p_3=0}^{\min(q_i,q_l)}\sum_{p_4=0}^{\min(n_j,n_k)}\sum_{p_5=0}^{\min(m_j,m_k)}\sum_{p_6=0}^{\min(q_j,q_k)} p_1!p_2!p_3!p_4!p_5!p_6!\binom{n_i}{p_1}\binom{n_l}{p_1}\binom{m_i}{p_2}\binom{m_l}{p_2} \\ & \times \binom{q_i}{p_3}\binom{q_l}{p_3}\binom{n_j}{p_4}\binom{n_k}{p_4}\binom{m_j}{p_5}\binom{m_k}{p_5}\binom{q_j}{p_6}\binom{q_k}{p_6}(-1)^{u+v/2+n_j+m_j+q_j+n_k+m_k+q_k}\left(\frac{1}{2}\right)^u x^{u+1/2} \\ & \times \frac{\Gamma\left(\frac{1+2u+v}{2}\right)\Gamma(1+u)\Gamma\left(\frac{1+v}{2}\right)}{\Gamma\left(\frac{3+2u+v}{2}\right)}{}_2F_1\left(1+u,\frac{1+2u+v}{2};\frac{3+2u+v}{2};1-x\right),\end{aligned} \tag{13}$$

where we define $u=m_i+m_j+n_l+n_k-(p_1+p_2+p_4+p_5)$, $v=(q_i+q_l+q_j+q_k)-2(p_3+p_6)$, $R_L=(m_i+m_j)-(n_i+n_j)=-(\ell_{z,i}+\ell_{z,j})$, $R_R=(m_l+m_k)-(n_l+n_k)=-(\ell_{z,l}+\ell_{z,k})$, $x\equiv\omega_z/\omega_h$, and ${}_2F_1$ is the hypergeometric function. The δ functions $\delta_{q_i+q_j+q_l+q_k,\rm even}$ and δ_{R_L,R_R} in the formulation ensure the conservation of the parity with respect to z axis and the z component of angular momentum of system L_z, respectively. The formulation of Eq. (13) is confirmed by computing the Coulomb integral numerically.

For short NWQDs with $a<1$, the formulations of the Coulomb matrix elements are obtained by simply taking Euler's hypergeometric transformation for the hypergeometric function in Eq. (13), i.e., replacing

$${}_2F_1\left(1+u,\frac{1+2u+v}{2};\frac{3+2u+v}{2};1-x\right) \tag{14}$$

by

$$x^{-1+2u+v/2}{}_2F_1\left(\frac{1+v}{2},\frac{1+2u+v}{2};\frac{3+2u+v}{2};1-\frac{1}{x}\right). \tag{15}$$

The generalized formulations for the Coulomb matrix elements based on the 3D asymmetric parabolic model are probably derived, which allows for straightforward implementation of the CI theory and is widely applicable to arbitrary 3D confining semiconductor nanostructures.

C. Numerical approach

Based on the CI theory presented above, we follow the standard numerical direct diagonalization procedure to calculate the energy spectrum of N_e interacting electrons in a NWQD.[19] The numerically exact results are obtained by increasing the numbers of chosen single-electron orbital basis

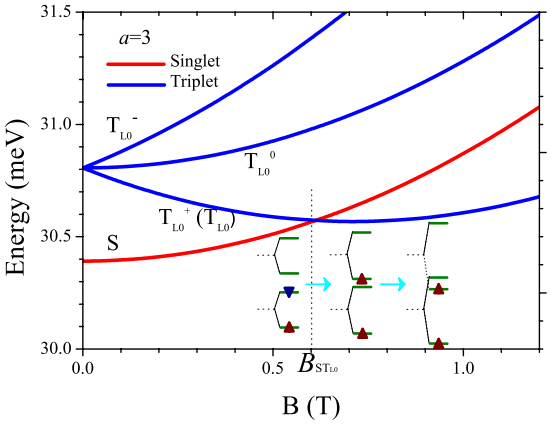

FIG. 3. (Color online) Magnetoenergy spectrum of two interacting electrons in a NWQD with transverse confining strength $\hbar\omega_0 = 13.3$ meV and aspect ratio $a=3$.

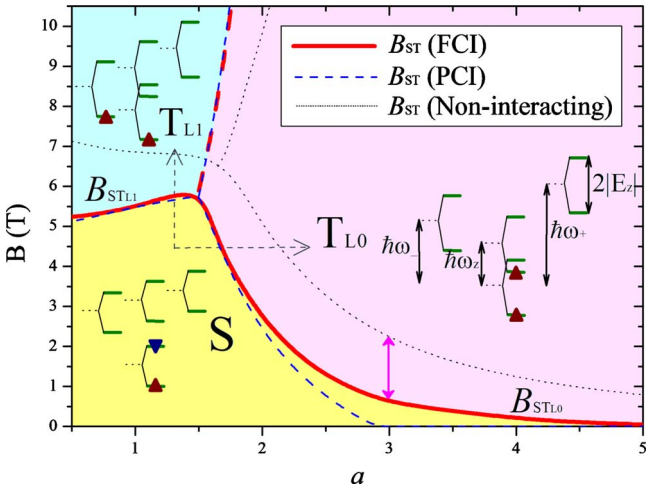

FIG. 4. (Color online) Spin-state diagrams of two-electron NWQDs of lateral confinement $\hbar\omega_0 = 13.3$ meV with respect to tunable magnetic field B and aspect ratio a. The states are distinguished by the curves of critical magnetic field $B_{ST_{L_z}}$ obtained from noninteracting (black dotted), PCI (blue dashed), and FCI (red solid) calculations.

and the corresponding N_e-electron configurations until a numerical convergence is achieved.

A convergence test was performed by applying the CI code to a previously studied case of 2D QD in Refs. 26 and 27 [by setting $l_z \to 0$ or $\omega_z \to \infty$ in Eq. (11)] and making a quantitative comparison with the given analytical result. For the studied 2D QD with lateral confining strength $\hbar\omega_0 = 2$ Ryd* (Ryd* being the effective Rydberg energy), the energy of the 2e ground state is exactly 6 Ryd*. Under the consideration of 26 single-particle orbitals and the 325 constructed 2e configurations, the calculated energies of the 2e ground states by our CI code show satisfactory high accuracy within the relative error ~0.15% (to the 2e energy itself). In the full CI (FCI) calculation for a 2e problem, we thus usually take the number of single-electron orbitals from 20 to 26 and that of the corresponding 2e configurations from 190 to 325.

III. NUMERICAL RESULTS AND DISCUSSION

A. Magnetic field induced ST transitions

Let us first consider two interacting electrons in a rodlike NWQD with the aspect ratio $a=3$ and the transverse confining strength $\hbar\omega_0 = 13.3$ meV using FCI calculation. The low-lying magnetoenergy spectrum of the two-electron NWQD is shown in Fig. 3, which consists of a spin-singlet state branch, labeled by S, and three triplet state branches split by the spin-Zeeman energy, labeled by T_{L0}^+, T_{L0}^0, and T_{L0}^- according to the z component of total spin ($S_z=+1$, $S_z=0$, and $S_z=-1$), respectively.[18,28] Since usually only triplet states with $S_z=+1$ are involved in ST transitions, we shall use $T_{L|L_z|}$ to denote the triplet states with angular momentum L_z throughout this paper, skipping the superscript + of $T_{L|L_z|}^+$ for brevity.

The main configurations of the two-electron ground states around the critical magnetic field are schematically shown in the lower right corner of Fig. 3. In the weak magnetic field regime ($B < B_{ST_{L0}} \sim 0.6$ T), the two electrons in the NWQD mainly occupy the lowest s orbital simply following the Aufbau principle, and form a spin-singlet ground state. With increasing B, the triplet state T_{L0} is more energetically favorable than the singlet state because of the increasing spin-Zeeman energy, the reduced Coulomb repulsion, and exchange energy between the two spin-polarized electrons. A crossing of the singlet branch and the triplet state branch T_{L0} is observed at the critical magnetic field $B_{ST_{L0}} = 0.6$ T. Such magnetic field induced ST transitions are attributed to the energetic competition between single-particle energy quantization, the spin-Zeeman energy, and the Coulomb interactions including the direct, exchange, and correlation interactions as well.[10]

Other weak spin-related terms, such as the spin-orbital coupling (SOC) with one to two orders of magnitude smaller than the kinetic quantization of QD are neglected in the Hamiltonian of Eq. (11). The SOC mixes the spin of the S and T_{L0} states and creates an anticrossing of the S and T_{L0} branches around the $B_{ST_{L0}}$ with a small energy gap, typically only ~0.1–0.5 meV as observed in previous experiments.[18]

B. Geometry- and *B*-controlled state transitions

Figure 4 shows the calculated spin-state diagrams of the two-electron ground state of the NWDQs with a fixed cross-section diameter (fixed $\hbar\omega_0 = 13.3$ meV) but various lengths (various $\hbar\omega_z$) with respect to the applied magnetic field B and the aspect ratio a. Three states (S, T_{L0}, and T_{L1}) are distinguished by the curves of critical magnetic fields B_{ST} in Fig. 4. Correspondingly, the main configurations of the 2e ground states are depicted inside the colored regions of the states. To identify the various underlying mechanisms in the state diagrams, including the spin-Zeeman effect and the interparticle Coulomb interactions, the spin-state diagrams are calculated by using noninteracting, full CI, and partial CI calculations, respectively.

In the noninteracting calculation, the Coulomb interactions are artificially disabled and the considered ST transi-

tions are induced only by the spin-Zeeman effect. The comparison between the results of non-interacting model and FCI calculations allows us to distinguish effects of the Coulomb interaction and spin-Zeeman coupling on the ST transitions. In particular, to highlight the Coulomb correlation effect, a partial CI (PCI) calculation is also performed for the spin-state diagrams, in which only the lowest-energy configuration is taken as the sole basis and the couplings from higher-energy configurations are excluded.

The essential features of the state diagrams can be realized based on the NI picture. For a not very long (small or moderate a) NWQD with weak B, the 2e ground state is likely to be the spin-singlet state S, simply following Aufbau principle (the yellow region labeled by S in the left-lower corner of Fig. 4). Starting from the singlet state S, the two-electron ground state of a NWQD might be switched to the spin-triplet states (the pink region T_{L0} or the cyan region T_{L1}) by increasing either a or B (see the horizontal and vertical dashed lines with arrows in Fig. 4 for the guidance of eyes).

Following the horizontal dashed line, the longitudinal energy quantization $\hbar\omega_z$ is decreased by the increase in a. With the addition of spin-Zeeman term, the spin-up level of p^0 orbital could become even lower than the spin-down level of s orbital if the decreasing $\hbar\omega_z$ is so small as that $\hbar\omega_z < 2|E_z|$ (see the difference between the schematic configurations for the S and T_{L0} states). In this situation, the 2e ground state can transit to the spin-triplet states T_{L0}, simply following spin Pauli exclusion principle. The critical magnetic field $B^0_{ST_{L0}}$ for the S-T_{L0} transition in the noninteracting case can be expressed as

$$B^0_{ST_{L0}} = \frac{\hbar\omega_0}{a^2|g^*|\mu_B}, \tag{16}$$

showing a quadratic decay with a (see Appendix for detailed derivation), as observed in Fig. 4. On the other hand, the transition of a 2e ground state of NWQD from the singlet state S to the triple one T_{L1} is shown also possible by increasing the strength of applied magnetic field. Following the vertical dashed line, increasing B reduce the energy separation between the s and p^- orbital levels, i.e., $\hbar\omega_-$. Similar to the case of S-T_{L0} transition, a S-T_{L1} transition can happen as the decreased $\hbar\omega_-$ is so small as that $\hbar\omega_- < 2|E_z|$. For non-interacting cases, the critical magnetic field $B^0_{ST_{L1}}$ for the S-T_{L1} transitions can be explicitly expressed as

$$B^0_{ST_{L1}} = \frac{\hbar\omega_0}{\sqrt{|g^*|\mu_B(|g^*|\mu_B + 2\mu_B^*)}}, \tag{17}$$

where $\mu_B^* \equiv e\hbar/2m^*$(see Appendix). Thus, for a QD with a fixed $\hbar\omega_0$, the $B^0_{ST_{L1}}$ remains nearly constant, but slightly varies with a due to the a-dependent feature of the effective g-factor g^* [see Eq. (10)], as observed in Fig. 4.

The Coulomb interactions are shown to reduce the singlet state area in the diagrams from the comparison between the noninteracting and CI results. For example, the segment of vertical solid line at $a=3$ in Fig. 4 indicates that the critical magnetic field is significantly reduced from $B_{ST_{L0}} \approx 2.3$ T (for the noninteracting case) to 0.6 T (for the FCI case) as the Coulomb interactions are taken into account. The negative exchange interaction and the reduced Coulomb repulsion in the T_{L0} state lead to the reduction in the strength of the interacting critical magnetic field B_{ST_0}, which can be estimated by Eq. (A9) shown in Appendix. We also notices that the $B_{ST_{L1}}$ for the S-T_{L1} transitions increases slightly with increasing a because the strength of Coulomb interaction is reduced by the increase in dot volume.

Basically, the results obtained from the FCI and PCI calculations have similar features except for those in the regime of high a ($a>3$). While the PCI calculation shows the vanishing $B_{ST_{L0}}$ for $a \sim 3$, the FCI calculation yields the always nonzero $B_{ST_{L0}}$. This means that the Coulomb correlations energetically favor the spin-singlet state as ground state and become more pronounced in long NWQDs. This is because the number of the singlet configurations (with the additional paired electron filling in the same orbital) involved in the 2e ground states is more than that of the triplet ones and the singlet states retain more Coulomb correlation to lower their energies.

C. Crossover from disklike to rodlike QDs

The spin-state diagrams of Fig. 4 suggest that purposely accessing a specific spin state of two electron is feasible through the geometrical control of NWQDs. For instance, the ground state of a two-electron NWQD can be switched from the singlet S to the triplet state T_{L0} by increasing the aspect ratio a at the fixed $B=5$ T (trace the horizontal dashed line in Fig. 4). Such a geometrical control of NWQD could be achieved by the delicate control of the length of a heterostructured NWQD in the growth process (ω_z control) (Ref. 17) or by the electrical control of the patterned electrodes on a NWQD (control of both ω_0 and ω_z).[18]

Figure 5 presents the spin-state diagrams of two-electron NWQDs with respect to the lateral and longitudinal confinements, parametrized by $\hbar\omega_0$ and $\hbar\omega_z$, respectively, in a fixed magnetic field $B=5$ T for (a) noninteracting two electrons with $g^* \neq 0$, (b) interacting two electrons with $g^* \neq 0$, and (c) interacting two electrons with $g^*=0$. In Figs. 6(a) and 6(b), we present the relevant two-electron configurations to the spin-state diagrams of Figs. 5(a) and 5(b) with the inclusion of spin-Zeeman effect ($g^* \neq 0$), while in Figs. 6(c) and 6(d) we present the relevant two-electron configurations to the spin-state diagrams of Fig. 5(c) for $g^*=0$

The noninteracting spin-state diagram is first shown in Fig. 5(a) in order to identify the spin-Zeeman effect and also contrast the Coulomb interaction effects on the interacting spin-state diagrams presented in Fig. 5(b). In the noninteracting case, the features of the spin states of Fig. 5(a) are purely determined by the competition between geometry-dependent quantized electronic structures of dots and the spin-Zeeman splitting, which is nearly a constant here created by the fixed B. Three distinctive spin states, S, T_{L0}, and T_{L1}, are marked in different colors in Fig. 5(a). In the yellow region (denoted by S) where both $\hbar\omega_0$ and $\hbar\omega_z$ are large, the kinetic quantizations in both longitudinal and lateral directions are stronger than the spin-Zeeman splitting and S remains as a ground

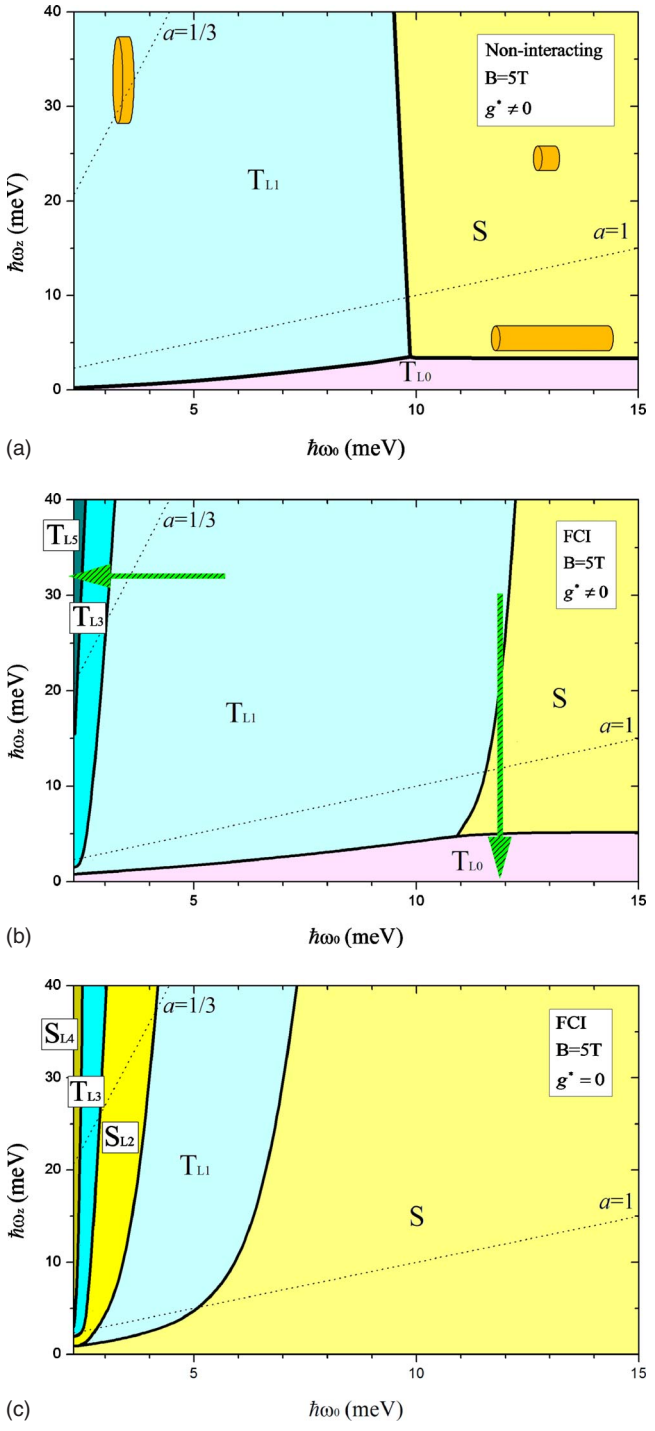

FIG. 5. (Color online) Spin-state diagrams of doubly charged NWQDs with respect to the lateral and longitudinal confinements, parametrized by $\hbar\omega_0$ and $\hbar\omega_z$, respectively, in a fixed magnetic field $B=5$ T for (a) noninteracting two electrons with $g^*\neq 0$, (b) interacting two electrons with $g^*\neq 0$, and (c) interacting two electrons with $g^*=0$.

state. Reducing the longitudinal confinement, $\hbar\omega_z$, can lead to the S-T_{L0} [from the yellow S region to the pink T_0 one] transition as $\hbar\omega_z \lesssim 2|E_Z|$. Similarly, reducing the transverse confinement leads to the S-T_{L1} transition as $\hbar\omega_- \lesssim 2E_Z$ (from the yellow S to the light cyan T_{L1} region). The feature of the

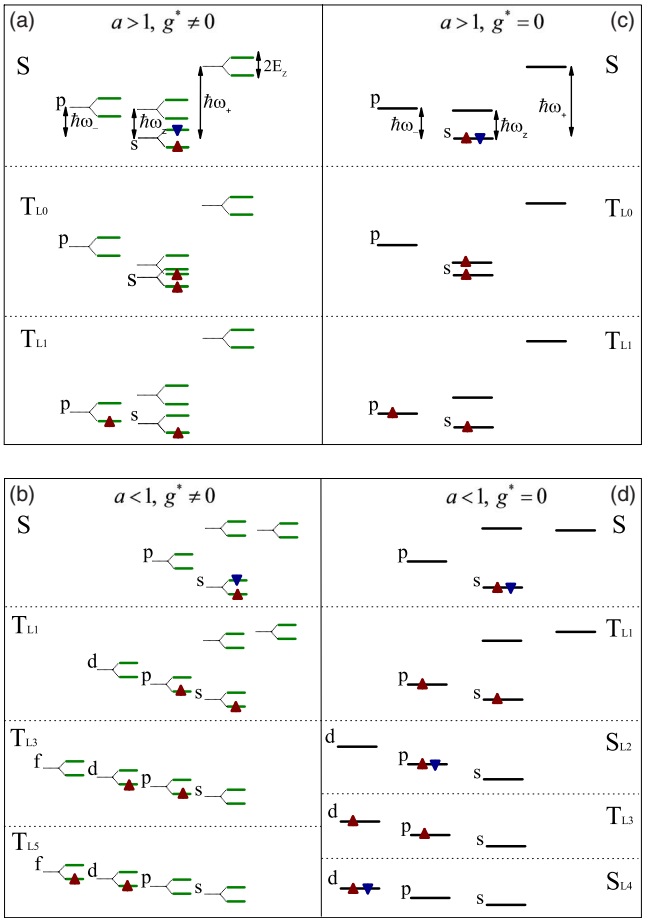

FIG. 6. (Color online) Relevant two-electron configurations possibly being the main components in the ground states of NWQDs in an uniform magnetic field $B=5$ T for (a) $a>1$ and $g^*\neq 0$, (b) $a<1$ and $g^*\neq 0$, (c) $a>1$ and $g^*=0$, and (d) $a<1$ and $g^*=0$.

spin-state diagram for noninteracting NWQDs in Fig. 5(a) can be well described by derived formulations Eqs. (A4a)–(A4c) shown in Appendix. For example, Eq. (A4a) shows that as the S-T_0 transitions occur the critical longitudinal confinement strength $\hbar\omega_z$ of a NWQD is independent of the transverse confinement $\hbar\omega_0$, shown as a horizontal line separating the S and T_{L0} regimes in Fig. 5(a).

Compared with Fig. 5(a), the interacting spin-state diagram of Fig. 5(b) shows the following additional features: (i) larger areas of both T_{L0} and T_{L1} states are observed because of the additional negative exchange energies and the reduced direct Coulomb repulsions gained by the triplet states. (ii) A NWQD with $\hbar\omega_0 \approx 12$ meV could experience a three-state transitions from T_{L1} (cyan) to S (yellow), and then to T_{L0} (pink) with increasing the length of wire, from $\hbar\omega_z > 25$ meV to $\hbar\omega_z < 5$ meV [see the vertical line positioned at $\hbar\omega_0 = 12$ meV in Fig. 5(b)].

(iii) In the regime of small $\hbar\omega_0$ and large $\hbar\omega_z$ (i.e., flat quasi-2D dots with $a \ll 1$), a series of transitions from the spin-singlet states to various triplet states, T_{L1}, T_{L3}, T_{L5}, etc. [see Fig. 6(b)] and a staircase increase in total orbital angular momentum are observed with reducing the lateral confinement $\hbar\omega_0$.

In the weak laterally confining regime, few electrons in the quasi-2D QD in a high magnetic field successively fill

the orbitals with negative z projection of orbital angular momentum, i.e., the orbitals of lowest Landau level (LLL), with small kinetic-energy separation $\hbar\omega_-$. The interparticle Coulomb interactions thus become particularly pronounced among the particles on the nearly degenerate LLL orbitals with almost quenched kinetic energies. In order to minimize the Coulomb repulsion, the particles on the quasidegenerate orbitals tend to spread the occupancy of orbitals as far as possible, but in competition with the cost of increase in kinetic energy. As a result, with reducing $\hbar\omega_0$ or increasing B, the total angular momentum of two electron increases, as previously discussed by Wagner *et al.*[9] for gated 2D QDs.

Figure 5(c) shows the spin-state diagram of two interacting electrons calculated by FCI method but with the vanishing spin-Zeeman term, i.e., $g^*=0$. This allows us to distinguish the effects of spin-Zeeman energy and the Coulomb interactions on the spin-state diagram of Fig. 5(b), and also to study the spin states of QD made of a material with small g^* such as GaAs. Without spin-Zeeman splitting, the significant features of Fig. 5(c) are completely determined by the many-body effects and geometry-engineered electronic structures of NWQDs.

In the $a>1$ regime, unlike the result shown in Fig. 5(b), the T_{L0} regime disappears and naturally there is no S-T_{L0} transition observed. This is because the Coulomb correlations that energetically favor spin-singlet state as mentioned previously, become dominant and compensate the negative exchange energy gained by the T_{L0} states.[6,28] However, in the small $\hbar\omega_0$ regime, an additional ST state oscillation with decreasing $\hbar\omega_0$ is observed. Compared with Fig. 5(b), the difference is the emergencies of various singlet states between the triplet states. This is due to the removal of spin-Zeeman splittings, which energetically favor only the triplet states. Such a ST state oscillation is evidenced as a main feature of a flat 2D QD with small spin-Zeeman effect, as shown both theoretically[9] and experimentally[12] in the previous studies.

IV. SUMMARY

In conclusion, we present a theoretical study of spin-state transitions of two electrons confined in nanowire quantum dots with highly tunable aspect ratio and external magnetic field along the principal axis of wire. A configuration-interaction theory based on a 3D parabolic model for such three-dimensionally confining QDs is developed for the study, which provides generalized explicit formulation of the Coulomb matrix elements and allows for straightforward implementation of direct diagonalization. The study reveals fruitful features of spin ST transitions with respect to the tunable geometric aspect ratio and applied magnetic field.

For disklike QDs, the ST transition behaviors may be dominated by the spin-Zeeman, the direct-Coulomb, and the exchange energies. The pronounced Coulomb correlations are identified in rodlike QDs with aspect ratio $a>3$, which energetically favor singlet-spin states and yield the always nonzero critical magnetic fields of ST transitions. The developed theory is further employed to study spin-state diagram in the dimensional crossover regime from the 2D (disklike) QDs to finite 1D (rodlike) QDs. In the 2D disklike QD regime, various distinctive spin states are emerged under the conditions of appropriate lateral confinement strength and magnetic fields. In the rodlike QD regime, switching the ST transitions is shown feasible by controlling both lateral and/or longitudinal confinement strength.

ACKNOWLEDGMENTS

This work was financially supported by the National Science Council in Taiwan through Contracts No. NSC-98-2112-M-009-011-MY2 (S.J.C.) and No. NSC97-2112-M-239-003-MY3 (C.S.T.). The authors are grateful to the facilities supported by the National Center of Theoretical Sciences in Hsinchu and the National Center for High-Performance Computing in Taiwan.

APPENDIX: ANALYSIS OF CRITICAL MAGNETIC FIELD OF SPIN-STATE TRANSITION

1. Noninteracting cases

The total energies of the noninteracting 2e S and the triplet (T_{L0} and T_{L1}) states are explicitly given by

$$E_S^0 = \hbar\omega_+ + \hbar\omega_- + \hbar\omega_z, \tag{A1a}$$

$$E_{T_{L0}}^0 = \hbar\omega_+ + \hbar\omega_- + 2\hbar\omega_z - 2|E_Z|, \tag{A1b}$$

$$E_{T_{L1}}^0 = \hbar\omega_+ + 2\hbar\omega_- + \hbar\omega_z - 2|E_Z|. \tag{A1c}$$

Defining $\Delta_{IJ}^0 \equiv E_J^0 - E_I^0$ as the energy difference between the noninteracting 2e states denoted by J and I, we derive

$$\Delta_{ST_{L0}}^0 = \hbar\omega_z - 2|E_Z|, \tag{A2a}$$

$$\Delta_{ST_{L1}}^0 = \hbar\omega_- - 2|E_Z|, \tag{A2b}$$

$$\Delta_{T_{L0}T_{L1}}^0 = \hbar\omega_- - \hbar\omega_z. \tag{A2c}$$

The above equations allow us to derive the critical magnetic fields B_{IJ}^0 for the state transitions in the noninteracting cases by setting $\Delta_{ab}^0=0$, given by

$$B_{ST_{L0}}^0 = \frac{\hbar\omega_0}{a^2|g^*|\mu_B}, \tag{A3a}$$

$$B_{ST_{L1}}^0 = \frac{\hbar\omega_0}{\sqrt{|g^*|\mu_B(|g^*|\mu_B + 2\mu_B^*)}}, \tag{A3b}$$

$$B_{T_{L0}T_{L1}}^0 = \frac{\hbar\omega_0}{2\mu_B^*}\left(a^2 - \frac{1}{a^2}\right), \tag{A3c}$$

where $\mu_B^* \equiv \hbar e/2m^*$. Equations (A3a)–(A3c) serve to account for the basic feature of Fig. 4.

For more illustration of Fig. 5(a), one can reformulate Eqs. (A3a)–(A3c) as

$$\hbar\omega_z = |g^*|\mu_B B_{ST_{L0}}^0, \tag{A4a}$$

$$\hbar\omega_0 = \sqrt{|g^*|\mu_B(|g^*|\mu_B + 2\mu_B^*)}B^0_{\mathrm{ST_{L1}}}, \tag{A4b}$$

$$\hbar\omega_z = \hbar\left[\sqrt{\omega_0^2 + \left(\frac{eB^0_{\mathrm{T_{L0}T_{L1}}}}{2m^*}\right)^2} - \frac{eB^0_{\mathrm{T_{L0}T_{L1}}}}{2m^*}\right], \tag{A4c}$$

which present the $\hbar\omega_0$-$\hbar\omega_z$ relationships for the spin-state transitions, and set $B^0_{\mathrm{IJ}}=5$ T as the applied magnetic field considered in the figure.

2. Two-orbital approximation for interacting cases

In the PCI scheme based on the two lowest orbitals, the total energies of the interacting 2e states are approximately

$$E_{\mathrm{S}} \approx E^0_{\mathrm{S}} + V^{ss}_{\mathrm{dir}}, \tag{A5a}$$

$$E_{\mathrm{T_{L0}}} \approx E^0_{\mathrm{T_{L0}}} + V^{sp^0}_{\mathrm{dir}} - V^{sp^0}_{\mathrm{ex}}, \tag{A5b}$$

$$E_{\mathrm{T_{L1}}} \approx E^0_{\mathrm{T_{L1}}} + V^{sp^-}_{\mathrm{dir}} - V^{sp^-}_{\mathrm{ex}}, \tag{A5c}$$

where

$$V^{ss}_{\mathrm{dir}} \equiv \langle 000;000|V|000;000\rangle, \tag{A6a}$$

$$V^{sp^0}_{\mathrm{dir}} \equiv \langle 000;001|V|001;000\rangle, \tag{A6b}$$

$$V^{sp^-}_{\mathrm{dir}} \equiv \langle 000;010|V|010;000\rangle, \tag{A6c}$$

$$V^{sp^0}_{\mathrm{ex}} \equiv \langle 000;001|V|000;001\rangle, \tag{A6d}$$

$$V^{sp^-}_{\mathrm{ex}} \equiv \langle 000;010|V|000;010\rangle. \tag{A6e}$$

Here the subscript "dir" (ex) is used for the matrix elements of direct (exchange) Coulomb interaction and the superscripts (ss, sp^0, sp^-, etc.) indicate the involved orbitals in the Coulomb interaction. After some algebra, the energy differences between the interacting 2e states can be obtained,

$$\Delta_{\mathrm{ST_{L0}}} \approx \Delta^0_{\mathrm{ST_{L0}}} - \delta\Delta_{\mathrm{ST_{L0}}}, \tag{A7a}$$

$$\Delta_{\mathrm{ST_{L1}}} \approx \Delta^0_{\mathrm{ST_{L1}}} - \delta\Delta_{\mathrm{ST_{L1}}}, \tag{A7b}$$

$$\Delta_{\mathrm{T_{L0}T_{L1}}} \approx \Delta^0_{\mathrm{T_{L0}T_{L1}}} - \delta\Delta_{\mathrm{T_{L0}T_{L1}}}. \tag{A7c}$$

Here $\delta\Delta_{\mathrm{IJ}}$ are defined as the decrease in Coulomb interaction energy as the 2e state transits from I to J and explicitly given by

$$\delta\Delta_{\mathrm{ST_{L0}}} = (V^{ss}_{\mathrm{dir}} - V^{sp^0}_{\mathrm{dir}}) + V^{sp^0}_{\mathrm{ex}}, \tag{A8a}$$

$$\delta\Delta_{\mathrm{ST_{L1}}} = (V^{ss}_{\mathrm{dir}} - V^{sp^-}_{\mathrm{dir}}) + V^{sp^-}_{\mathrm{ex}}, \tag{A8b}$$

$$\delta\Delta_{\mathrm{T_{L0}T_{L1}}} = (V^{sp^0}_{\mathrm{dir}} - V^{sp^-}_{\mathrm{dir}}) + (V^{sp^-}_{\mathrm{ex}} - V^{sp^0}_{\mathrm{ex}}). \tag{A8c}$$

A positive (negative) $\delta\Delta_{\mathrm{IJ}}$ indicates that the total Coulomb interaction energy is decreased (increased) as the 2e QD transits from the state I to the one J. Taking into account the Coulomb correction terms, Eqs. (A8a)–(A8c), the critical magnetic field $B_{\mathrm{ST_{L0}}}$ for the interacting 2e QDs can be expressed as

$$B_{\mathrm{ST_{L0}}} \approx B^0_{\mathrm{ST_{L0}}} - \delta B_{\mathrm{ST_{L0}}}, \tag{A9}$$

where $\delta B_{\mathrm{ST_{L0}}} = \delta\Delta_{\mathrm{ST_{L0}}}/(|g^*|\mu_B)$. Following Eqs. (A9), we examine the NWQD with $a=3$ shown in Fig. 4 with the Coulomb matrix elements $V^{ss}_{\mathrm{dir}}=3.0$ meV, $V^{sp^0}_{\mathrm{dir}}=2.2$ meV, and $V^{sp^0}_{\mathrm{ex}}=0.8$ meV and obtain $\delta\Delta_{\mathrm{ST_{L0}}}=1.6$ meV>0. Accordingly, the reduction in critical magnetic field due to the Coulomb interactions is estimated as $\delta B_{\mathrm{ST_{L0}}}\approx 2.3$ T, which is well consistent with the noninteracting and the PCI results shown in Fig. 4. Similarly, according to Eq. (A7c) one can derive

$$B_{\mathrm{T_{L0}T_{L1}}} \approx \frac{\hbar\omega_0}{2\mu_B^*}\left(a^{*2} - \frac{1}{a^{*2}}\right), \tag{A10}$$

where $a^* = a/\sqrt{(1+\delta\Delta_{\mathrm{T_{L0}T_{L1}}}a^2/\hbar\omega_0)}$. For rodlike NWQDs ($a>1$) where $\delta\Delta_{\mathrm{T_{L0}T_{L1}}}<0$ and $a^*>a$, we have $B_{\mathrm{T_{L0}T_{L1}}} > B^0_{\mathrm{T_{L0}T_{L1}}}$. The increase in the critical magnetic field by the Coulomb effect is clearly shown in Fig. 4.

*sjcheng@mail.nctu.edu.tw
†cstang@nuu.edu.tw

[1] J. R. Petta, A. C. Johnson, J. M. Taylor, E. A. Laird, A. Yacoby, M. D. Lukin, C. M. Marcus, M. P. Hanson, and A. C. Gossard, Science **309**, 2180 (2005).
[2] D. Loss and D. P. DiVincenzo, Phys. Rev. A **57**, 120 (1998).
[3] J. Fischer, M. Trif, W. A. Coish, and D. Loss, Solid State Commun. **149**, 1443 (2009).
[4] L. P. Kouwenhoven, T. H. Oosterkamp, M. W. S. Danoesastro, M. Eto, D. G. Austing, T. Honda, and S. Tarucha, Science **278**, 1788 (1997).
[5] L. P. Kouwenhoven, D. G. Austing, and S. Tarucha, Rep. Prog. Phys. **64**, 701 (2001).
[6] S. M. Reimann and M. Manninen, Rev. Mod. Phys. **74**, 1283 (2002).
[7] C. Ellenberger, T. Ihn, C. Yannouleas, U. Landman, K. Ensslin, D. Driscoll, and A. C. Gossard, Phys. Rev. Lett. **96**, 126806 (2006).
[8] J. Kyriakidis, M. Pioro-Ladriere, M. Ciorga, A. S. Sachrajda, and P. Hawrylak, Phys. Rev. B **66**, 035320 (2002).
[9] M. Wagner, U. Merkt, and A. V. Chaplik, Phys. Rev. B **45**, 1951 (1992).
[10] P. Hawrylak, Phys. Rev. Lett. **71**, 3347 (1993).
[11] B. Partoens, A. Matulis, and F. M. Peeters, Phys. Rev. B **59**, 1617 (1999).
[12] Y. Nishi, Y. Tokura, J. Gupta, G. Austing, and S. Tarucha, Phys.

Rev. B **75**, 121301(R) (2007).
[13] C. Fasth, A. Fuhrer, M. T. Björk, and L. Samuelson, Nano Lett. **5**, 1487 (2005).
[14] A. Pfund, I. Shorubalko, R. Leturcq, and K. Ensslin, Appl. Phys. Lett. **89**, 252106 (2006).
[15] A. Pfund, I. Shorubalko, K. Ensslin, and R. Leturcq, Phys. Rev. Lett. **99**, 036801 (2007).
[16] M. T. Björk, C. Thelander, A. E. Hansen, L. E. Jensen, M. W. Larsson, L. R. Wallenberg, and L. Samuelson, Nano Lett. **4**, 1621 (2004).
[17] M. T. Björk, A. Fuhrer, A. E. Hansen, M. W. Larsson, L. E. Fröberg, and L. Samuelson, Phys. Rev. B **72**, 201307(R) (2005).
[18] C. Fasth, A. Fuhrer, L. Samuelson, V. N. Golovach, and D. Loss, Phys. Rev. Lett. **98**, 266801 (2007).
[19] A. Wensauer, M. Korkusiński, and P. Hawrylak, Solid State Commun. **130**, 115 (2004).
[20] M. Dineykhan and R. G. Nazmitdinov, Phys. Rev. B **55**, 13707 (1997).
[21] J. T. Lin and T. F. Jiang, Phys. Rev. B **64**, 195323 (2001).
[22] W. Zhu and S. B. Trickey, Phys. Rev. A **72**, 022501 (2005).
[23] M. T. Björk, B. J. Ohlsson, C. Thelander, A. I. Persson, K. Deppert, L. R. Wallenberg, and L. Samuelson, Appl. Phys. Lett. **81**, 4458 (2002).
[24] C. Hermann and C. Weisbuch, Phys. Rev. B **15**, 823 (1977).
[25] P. Hawrylak, Solid State Commun. **88**, 475 (1993).
[26] M. Taut, J. Phys. A **27**, 1045 (1994).
[27] S. Pittalis, E. Räsänen, and M. A. L. Marques, Phys. Rev. B **78**, 195322 (2008).
[28] R. Hanson, L. P. Kouwenhoven, J. R. Petta, S. Tarucha, and L. M. K. Vandersypen, Rev. Mod. Phys. **79**, 1217 (2007).